Fermi National Accelerator Laboratory

FN-334
8055.000

CURRENT CARRYING TARGETS AND MULTITARGET ARRAYS FOR HIGH LUMINOSITY SECONDARY BEAMS

J. A. MacLachlan
Fermi National Accelerator Laboratory, Batavia, Illinois 60510 USA

April 1982

Operated by Universities Research Association Inc. under contract with the United States Department of Energy

FN-334
8055.000
April 1982

Current Carrying Targets and Multitarget Arrays for High Luminosity Secondary Beams

J.A. MacLachlan

I. Introduction

The desire to maximize secondary production into a limited acceptance naturally leads to an attempt to realize as nearly as may be a point target. The primary beam is focused to a small spot on a short target; a reasonable interaction probability is obtained by using the densest available material. However, the number of interactions is limited by the thermal energy density which the target can sustain. Even a small fraction of the beam from a high energy accelerator can deplete the density of a heavy metal target several fold within the few microsecond duration of a fast beam spill[1]. If the target is to withstand successive spills, a lower limit yet is set on the primary beam brightness. Therefore, when there is adequate primary beam available and the concern is maximum production rather than maximum efficiency, it

can be effective to increase the interaction volume and employ special tactics to reduce the loss of targeting efficiency. This note examines three related schemes which combine production target and focusing functions.

All three schemes use in one way or another the axially symmetric focusing provided by a uniform current density flowing along the beam axis. The beam optical properties of such "current monopole" lenses[2] are discussed in the next section. Section III discusses current carrying targets which combine the functions of production and focusing of secondaries[3]. Section IV examines a separated function variant in which the focusing is provided by lithium lenses[4] interleaved with multiple targets[5]. By exciting the targets of the multiple target array described in Section IV with current opposite to that in the lenses one arrives at the alternating gradient target channel discussed in Section V[6].

In Section VII these schemes are compared to one another and to a short, dense target in the context of antiproton production by high energy protons. These illustrative examples have their origin in the Fermilab Tevatron I project[7]; however, the particular parameters do not apply directly to the current version[8]. Monte Carlo yield calculations including at least approximate optimization have been carried out for each scheme with plausible limits on parameters. Various engineering and materials problems related to practical implementation have only been noted in passing. For another application the comparison of the three schemes might work out differently; the earlier sections

are intended to be sufficiently general to facilitate the analogous comparison for other cases. Note in particular that no attention has been devoted to the case of like sign for primary and secondary beams. Similar tactics can be employed in that situation as well, but the problem is simpler because focusing of secondaries will not cause defocusing of the primary beam.

From the standpoint of material properties a light metal target seems attractive in several respects. First, dE/dx is lower so that the primary energy deposition is lowered. Likewise the energy deposited by heavy target fragments, which is distributed more or less the same way as the ionization loss, is much less for light nuclei. Furthermore, because the interaction length and radiation length are of the same order, the electromagnetic cascade does not develop very far. Finally, the heat capacity per unit volume is significantly higher. In fact, for beryllium not only the heat capacity but also the enthalpy reserve $\Delta H=\int_{T_o}^{T_F} c_p \, d_T$ between room temperature and the melting point is substantially greater than for the refractory heavy metals like tungsten[9]. The degree to which these advantages can be utilized to obtain greater production of secondaries depends on the degree to which the design of the secondary beam optics can circumvent the depth of field problem resulting from the increased interaction length characteristic of light metal targets. For large acceptance the depth of field is severely limited so that target length becomes a dominant parameter in determining the yield. For smaller acceptance the low-Z materials are relatively

more attractive because of their low multiple scattering and greater tolerance of intense primary beam.

The object of the targeting schemes developed below is to increase the effectiveness of low-Z material by circumventing the depth-of-field problem with special beam optics wherein target elements and focusing elements are combined or interleaved. The domain of primary and secondary beam parameters for which they may be advantageous is limited by beam optics and the feasibility of the focusing elements. Both of these limitations are explored in the following; the results appear relevant to high luminosity secondary beams such as that required for the Fermilab proton-antiproton colliding beam project[8].

II. Current Monopole Lenses

A cylindrical conductor carrying current uniformly distributed with density J_z [A/m^2] produces an azimuthal magnetic field with a constant radial gradient

$$\frac{\partial B_\theta}{\partial r} = \frac{\mu J_z}{2} \qquad (1)$$

where $\mu \tilde{=} \mu_o = 4\pi \times 10^{-7}$ [MKSA] and the subscripts refer to a cylindrical coordinate system with z-axis along the axis of the conductor. Because the Lagrangian is independent of time and

there is no electrostatic potential, the equations for the particle trajectories in the field can be obtained from a dimensionless "orbit Lagrangian"[10]

$$\Lambda = \frac{d\ell}{dz} + \frac{\vec{A}}{B\rho} \cdot \frac{d\vec{r}}{dz} \tag{2}$$

via the Lagrange equations

$$\frac{d}{dz}\frac{\partial \Lambda}{\partial r'} - \frac{\partial \Lambda}{\partial r} = 0$$

$$\frac{d}{dz}\frac{\partial \Lambda}{\partial \theta'} - \frac{\partial \Lambda}{\partial \theta} = 0 \tag{3a \& 3b}$$

where ℓ is the orbit length, $\vec{A}$ is the magnetic vector potential, and the primes indicate differentiation with respect to the independent variable z, the displacement along the reference trajectory. The vector potential giving B_θ is

$$A_z = -\frac{\mu J_z}{4} r^2. \tag{4}$$

The orbit Lagrangian for this potential written in cylindrical coordinates is

$$\Lambda = \sqrt{1+r'^2+r^2\theta'^2} - \frac{\mu J_z}{4B\rho} r^2. \tag{5}$$

The orbit equations become

$$r'' - r\theta'^2 + \frac{\mu J_z}{2B\rho} r = 0$$

and

$$\frac{d}{dz}(r^2\theta') = 0 \tag{6a \& 6b}$$

when all terms up to and including $O(r^2)$ are retained. All higher order terms are kinematic only, i.e., do not contain the potential. The second equation expresses the conservation of a quantity related to angular momentum about the z-axis so that

eq. 6a can be written

$$r'' - \frac{\lambda^2}{r^3} + k^2 r = 0 \tag{7}$$

where λ denotes the conserved $r^2\theta'$ and

$$k^2 = \frac{1}{B\rho}\frac{\partial B_\theta}{\partial r} = \frac{\mu J_z}{2B\rho} \tag{8}$$

is the focusing strength. To apply ordinary linear beam optics methods to eq. 6b it is necessary to ignore the λ-term or treat it as a perturbation. Writing λ in cartesian coordinates

$$\lambda = xy' - yx' \tag{9}$$

makes it clear that what one loses by dropping the λ term is the description of the helical trajectories of particles whose velocity vectors are not coplanar with the axis. In most applications it will be true that the primary beam emittance is relatively small and that the principal properties of the system

can be determined by treating only the on-axis production. In the examples treated in the final section of this note, the systems designed with the matrix methods are simulated in a Monte Carlo which includes the finite primary emittance as well as scattering by the lens material to provide detailed results for the phase space distributions of both the primary beam and secondary production.

III. Current Carrying Targets

An attractive application of the current monopole focusing is to run an electric current through a production target to focus the secondaries toward the beam axis[3]. This technique would seem to circumvent the depth-of-field problem by providing more focusing for production from the upstream end of the target. Consider, for example, the situation represented in Fig. 1 where the secondaries from the upstream end are focused on the downstream end of the target. The two ends appear as a single short source whereas all secondaries produced between them will leave the target at some angle less than their angle of production. Secondaries produced at the center will form a parallel beam.

If one supposes that the focusing target establishes potentially infinite depth-of-field, the appropriate length for the target is determined simply by maximizing

$$x_{abs} = \int_0^L e^{-s/\lambda}\, e^{-(L-s)/\bar{\lambda}}\, ds/\lambda = \begin{cases} \dfrac{e^{-L/\lambda} - e^{-L/\bar{\lambda}}}{\lambda/\bar{\lambda} - 1} & (\lambda \neq \bar{\lambda}) \\ \dfrac{L}{\lambda}\, e^{-L/\lambda} & (\lambda = \bar{\lambda}) \end{cases} \tag{10}$$

which integrates production and absorption over the target length L; λ and $\bar{\lambda}$ are respectively the primary and secondary particle absorption lengths. Taking the case $\lambda=\bar{\lambda}$, which is not too bad for low-Z materials, the optimum length is $L=\lambda$. While Figure 1 implies a choice of $\bar{k}L=n\pi$ where $\bar{k}$ is defined according to Eq. 8 with the magnetic rigidity $B\rho$ evaluated for the secondary beam momentum $\bar{p}$, in fact for $\bar{k}L>2\pi$ the value is no longer very critical. The choice of $\bar{k}$ depends rather on the acceptance and the production angles to be accommodated. Denoting the secondary beam transfer matrix through the target by $\bar{M}_{12}$ and its elements by $\bar{m}_{ij}$ one has

$$\bar{r} = \bar{m}_{12}\, \bar{\theta} = \frac{\sin \bar{k}L\ \bar{\theta}}{\bar{k}} \tag{11}$$

where $\bar{\theta}$ is the angle of a secondary produced on axis. Thus, to contain the production up to some maximum desired angle $\bar{\theta}_{max}$ entirely within the target calls for a target radius

$$r_t \geq \theta_{max}/\bar{k} \tag{12}$$

This minimum target radius determines the spatial component of the acceptance

$$\bar{\varepsilon} = \pi\theta_{max}\, r_t \tag{13}$$

so that using the equality in eq. 12

$$\bar{k} = \pi\, \theta^2_{max}/\bar{\varepsilon} \tag{14}$$

Taking a characteristic transverse momentum $\langle \bar{p}_\perp \rangle$ for the production process to set the desired angle

$$\theta_{max} \sim \frac{\langle \bar{p}_\perp \rangle}{\bar{p}} \tag{15}$$

fixes the value of $\bar{k}$. There are two further considerations which may lead to a different choice of $\bar{k}$ in practical cases. One is the constraint on $\bar{k}$ set by material properties and the other is

the defocusing of the primary beam by the target. It can be easily shown that the ultimate capability of a material as a linear lens is expressed most simply as the maximum surface magnetic field that may be sustained with uniform current distribution and does not depend on radius etc. so long as the application permits the excitation pulse length to be appropriately scaled to the radius and skin depth[11]. Since

$$\bar{k} = \frac{1}{(\overline{B\rho})} \frac{\partial B_\theta}{\partial r} = \frac{B_\theta(r=r_t)}{(\overline{B\rho})\ r_t} \tag{16}$$

eq. 14 requires

$$B_\theta(r=r_t) = (\overline{B\rho})\,\pi\ \bar{\theta}_{max}^3\ /\bar{\epsilon}\ , \tag{17}$$

a value which exceeds attainable fields by an order of magnitude for the example discussed in Section VI when θ_{max} is chosen according to eq. 15. Because of the cubic dependance on θ_{max}, however, one may not have to give up too much to attain a realizable system.

The defocusing of the primary beam depends on the primary momentum, the target length, and the gradient; it is a

counterproductive effect which leads to an optimum value of $\bar{K}$ which can be substantially smaller than that determined from eqs. 14 and 15 above. As indicated in Fig. 1 the primary beam should be focused to a waist at the center of the target. The transfer matrix from the center to the downstream end M_{02} with elements denoted by m_{ij} is

$$M_{02} = \begin{pmatrix} \cosh kL/2 & 1/k \sinh kL/2 \\ k \sinh kL/2 & \cosh kL/2 \end{pmatrix} \tag{18}$$

where $k=(\bar{p}/p)^{1/2} \bar{K}$. The β,α Twiss parameters at the downstream end of the target will be

$$\beta_2 = m_{11}^2\beta_0 + m_{12}^2/\beta_0$$
$$\alpha_2 = -m_{21}\, m_{11}\beta_0 - m_{12}\, m_{22}/\beta_0 \tag{19 \& 20}$$

One aims to have the primary beam as close to a pencil beam as possible, i.e., to have β_2 as close to β_0 as possible. Minimizing β_2 with respect to β_0 gives

$$\beta_0 = m_{12}/m_{11} = 1/k \tanh kL/2 \tag{21}$$

Achieving this β-value at center of the target requires focusing the primary beam very strongly. This focusing could itself be a significant constraint on the design; in which case one might choose β_0 to minimize the magnitude of $\alpha_1 = -\alpha_2$. Then,

$$\beta_0 = \sqrt{m_{12}\, m_{22}/(m_{21}\, m_{11})} = \frac{1}{k} \tag{22}$$

The result for the minimum β-variation case (eq. 21) is

$$\begin{aligned} \alpha_2 &= -\cosh kL \\ \beta_2 &= (1/k) \sinh kL \end{aligned} \qquad (\beta \text{ optimized}) \tag{23a}$$

and for the minimum convergence case (eq. 22)

$$\begin{aligned} \alpha_2 &= -\sinh kL \\ \beta_2 &= (1/k) \cosh kL \end{aligned} \qquad (\alpha \text{ optimized}) \tag{23b}$$

The primary beam is then matched to the target by focusing it so that for k=0 it would drift to a waist with $\beta=\beta^*$ a distance s downstream of the upstream end of the target:

$$\alpha_1 = -\alpha_2 = s/\beta^*$$

$$\beta_1 = \beta_2 = \beta^* + s^2/\beta^*$$

(24 & 25)

so that

$$s = -\beta_2/(\alpha_2+\alpha_2^{-1})$$

$$\beta^* = -s/\alpha_2$$

(26 & 27)

Eqn. 27 shows that for large k strong upstream focusing is required to bring the beam to a small β^*; in extreme cases the primary beam may need to be focused by a monopole lens, e.g., lithium lens.

An upper bound on the limit for $\bar{k}$ set by the defocusing of the primary beam may be found easily by requiring that the primary beam spot on the entrance and exit faces be no more than the width of the secondary acceptance ellipse at that point. Assuming for simplicity that one takes $\bar{k}L=n\pi$ so that the acceptance at target end will be upright, one requires

$$\sqrt{\frac{\varepsilon \beta_2}{\pi}} \leq \frac{\bar{\varepsilon}}{\pi \bar{\theta}_{max}}$$

(28)

Using the optimized β_2 from eq. 23a on the lefthand side and eq. 14 relating $\bar{\kappa}$, θ_{max}, and $\bar{\varepsilon}$ on the right-hand side

$$\frac{\varepsilon}{\pi q\bar{\kappa}} \sinh q\bar{\kappa}L < \frac{\bar{\varepsilon}}{\pi\bar{\kappa}}, \tag{29}$$

where q is the momentum ratio $\bar{p}/p < 1$. Thus, the limit on $\bar{\kappa}$ is

$$\bar{\kappa} < [\sinh^{-1}(q\bar{\varepsilon}/\varepsilon)]/qL \tag{30}$$

This criterion for $\bar{\kappa}$ is asserted to be an upper bound because no secondaries would be accepted from the production arising from primary particles outside the limit set in eq. 28. An optimization of yield vs. $\bar{\kappa}$ might disclose a lower optimum value.

The limit on current or B_{max} can be extended by operating the target in a fast pulsed mode in which the current flows almost entirely on the surface during the beam spill. In this case there is little disturbance to the primary beam within the target, but secondaries leaving the sides are bent toward the axis. For a given target diameter this clearly leads to a larger emittance because there is no focusing at all for secondaries which do not exit the side of the target. However, if the primary beam has sufficiently small emittance that the target diameter can be very

small, this mode could be competitive. Because the optics are not even approximately linear the general formulation has not been worked out and it is not easy to estimate the secondary beam phase space distribution. In Sec. VII the surface current mode is compared to the uniform current density mode at fixed target diameter, current, etc.

IV. Multiple Target Array

The combination of focusing and production target functions can lead to unphysical requirements on the material or to unacceptable performance compromises in certain applications. Elemental beryllium, for example, is rather brittle and may not be useable to as high an excitation as one would infer from its heat capacity and fusion temperature. The most complete development of current monopole lenses has been done on lithium lenses intended solely as focusing elements[1,2]; in the course of the development beryllium was tried and rejected because of breaking. It is a natural conceptual step from the current carrying target to the separated function arrangement shown in Fig. 2. This interleaved array of targets and lithium lenses[5] is arranged to provide a secondary beam focus in the center of each target so that each provides an identical short target emittance to the collection system.

The optimization of such an array consists primarily of maximizing the ratio of target length to lens lengths, having adequate angular aperture to match the secondary acceptance, and

matching target lengths to the secondary β-function at the waists, $\bar{\beta}_t$. This matching is in turn determined by the source width which will depend on the amount of primary beam defocusing. Clearly the first goal is to push things together as close as possible. The secondary beam transfer matrix for one cell of the array is

$$\bar{M}_{12} = \begin{pmatrix} 1 & \ell \\ 0 & 1 \end{pmatrix} \begin{pmatrix} \cos \bar{k}L & \frac{1}{\bar{k}} \sin \bar{k}L \\ -k \sin \bar{k}L & \cos \bar{k}L \end{pmatrix} \begin{pmatrix} 1 & \ell \\ 0 & 1 \end{pmatrix} = \begin{pmatrix} -1 & 0 \\ 0 & -1 \end{pmatrix} \tag{31}$$

The primary beam will have a waist in the center of the array and the matching primary beam is calculated as in Section III by calculating from the waist to the downstream end and using symmetry to get β_1 and α_1.

The maximum focusing capability of the collecting lenses is governed by the maximum sustainable field B_{max}. In the thin lens approximation

$$\frac{1}{\bar{f}} = \frac{2}{\bar{L}} + \frac{2}{\bar{L}} = \frac{B_{max}\ \ell}{B\bar{\rho}a} \tag{32}$$

where L is the cell length, ℓ the lens length and a the lens radius. The radius of the lens follows from angular acceptance

$$a \geq \bar{\theta}_{max}\ L/2 \tag{33}$$

The lens should be as short as possible to limit absorption of secondaries. Certainly one wants at least $\ell < L/2$; otherwise the ends of the lens would not have very much effect because of the small beam size near the target. Taking $\ell = L/2$,

$$\bar{\theta}_{max} = \frac{\bar{p}_{\perp}}{\bar{p}} = \frac{\bar{p}}{\overline{B\rho}/.03} , \tag{34}$$

and using eqs. 32 and 33 sets the approximate scale as

$$\frac{L}{2} = \ell = \frac{2\bar{p}_{\perp}}{.03\ B_{max}} \tag{35}$$

The thick lens transfer matrix (eq. 31) must be used to get the exact relations.

When the primary beam width is taken into account the secondary acceptance may be inadequate to provide angular acceptance of $\bar{\theta}_{max}$ determined by eq. 34. The final steps of optimizing consist of reducing $\bar{\theta}_{max}$ and consequently also reducing the required secondary focusing and resulting defocusing of the primary beam.

V. Alternating Gradient Target Channel

Unless the primary momentum is very much greater than the secondary momentum, the defocusing of the primary beam is the major limit to using long target systems including focusing for secondaries. By employing focusing elements of both signs it is possible to contain both beams in the manner of an alternating gradient accelerator or FODO beam channel[6]. Although the application is very different from accelerator design it will be convenient to pretend that the target channel structures are infinitely long and apply the Courant Snyder formalism. In practice, strictly stable solutions are not required, but solutions failing to meet the betatron oscillation stability criterion are unlikely to be satisfactory for more than a cell or two.

Figure 3 represents a single cell of a FODO target channel. The target lenses are focusing for the primary beam, the lithium lens is focusing for the secondaries. This polarity follows from the matching of target emittance to lattice functions, i.e., placing the target so that the secondaries emanate from a narrow waist. The fact that the primary beam is thus at its maximum width in the target limits the range of acceptable primary emittance and momentum.

Using a notation indicated in Fig. 3, the value of the lattice functions at the target waist are subscripted "T" and the values at the collecting lens waist are subscripted "C". Values applying to the secondary beam are identified by an overscore,

e.g., β_T. The transfer matrix for the half cell of length L between target and collector is

$$M_{TC} = \begin{pmatrix} (\beta_C/\beta_T)^{1/2} \cos \mu/2 & (\beta_T\beta_C)^{1/2} \sin \mu/2 \\ -(\beta_T\beta_C)^{1/2} \sin \mu/2 & (\beta_T/\beta_C)^{1/2} \cos \mu/2 \end{pmatrix} \tag{36}$$

where μ is the phase advance per cell. Denoting the elements of this matrix by m_{ij}

$$\beta_T = \sqrt{-\frac{m_{22}\, m_{12}}{m_{11}\, m_{21}}} \tag{37}$$

and

$$\sin^2 \mu/2 = - m_{12}\, m_{21}. \tag{38}$$

The same expressions apply identically to the secondary beam with the corresponding overscored quantities. The secondary beam source at the target has the width of the primary beam so that acceptance matching requires

$$\bar{\beta}_T/\beta_T = \epsilon/\bar{\epsilon} = \sqrt{\bar{m}_{22}\, \bar{m}_{12}\, m_{11}\, m_{21}/(m_{22}\, m_{12}\, m} \tag{39}$$

where ϵ and $\bar{\epsilon}$ are primary beam emittance and secondary acceptance respectively. Generally β_T, the primary momentum p, the secondary momentum $\bar{p}$, ϵ, and $\bar{\epsilon}$ will be fixed parameters. While the phase advance μ is not rigidly fixed it will be very strongly controlled by the fact that $\bar{\mu} \simeq \pi$, i.e., there should be very nearly point-to-point focusing between target lens centers. Thus, the primary adjustable parameters to get β, $\bar{\beta}$, and $\bar{\mu}$ are the two focusing strengths and the half cell length L.

The transfer matrix M_{TC} can be written in thin lens approximation as

$$M_{TC} \simeq \begin{pmatrix} 1 - L/T & L \\ \frac{1}{\bar{C}} - \frac{1}{\bar{T}} - \frac{L}{\bar{C}\bar{T}} & 1 + \frac{L}{\bar{C}} \end{pmatrix} \tag{40}$$

where T and C are respectively the target lens and collector lens focal lengths

$$T = (k_T^2 L_T)^{-1} \tag{41}$$

and

$$C = (k_C^2 L_C)^{-1}. \tag{42}$$

For the secondary beam transfer matrix one simply scales T and C by $q=\bar{p}/p<1$ so that

$$\bar{M}_{TC} \approx \begin{pmatrix} 1 + \frac{L}{qT} & L \\ \frac{1}{qT} - \frac{1}{qC} - \frac{L}{q^2CT} & 1 - \frac{L}{qC} \end{pmatrix} \tag{43}$$

Using these approximate matrix elements in eqs. 37 and 38

$$\sin \mu/2 = \sqrt{\frac{L}{T} - \frac{L}{C} + \frac{L^2}{TC}} \tag{44}$$

$$\beta_T = L\sqrt{\frac{1 + L/C}{(1-L/T)(L/T-L/C+L^2/CT)}} = \frac{L}{\sin \mu/2}\sqrt{\frac{1+L/C}{1-L/T}} \tag{45}$$

$$\sin \bar{\mu}/2 = \frac{L}{qC} - \frac{L}{qT} + \frac{L^2}{q^2CT} \tag{46}$$

$$\bar{\beta}_T = L\sqrt{\frac{1 - L/qC}{(1+L/qT)(L/gC-L/qT+L^2/q^2CT)}} = \frac{L}{\sin \mu/2}\sqrt{\frac{1-L/qC}{1+L/qT}} \tag{47}$$

These equations show that besides the scaling with the momentum there is a trivial scaling with L. For qC=L eq. 43 shows that sin $\mu/2=1$ and $\bar{\beta}_T=0$ regardless of T so that one can adjust the strength of the target lens to match β_T more or less independently of the strength of the collecting lens.

The length scaling noted above can be employed to introduce new variables, a scaled target lens strength

$$\tau=L/T \tag{48}$$

and a scaled collector lens strength

$$\gamma=L/C \tag{49}$$

so that from eq. 40 for $\bar{M}_{TC}$ and the corresponding expression for the transfer matrix for the next half cell from collecting lens to target one has for the full cell transfer matrix of the secondary beam

$$\bar{M}_{TCT} = \begin{pmatrix} 1 + 2\left(\frac{\tau}{q} - \frac{\gamma}{q} - \frac{\gamma\tau}{q^2}\right) & 2L\left(1 - \frac{\gamma}{q}\right) \\ \frac{2}{L}\left(1 + \frac{\tau}{q}\right)\left(\frac{\tau}{q} - \frac{\gamma}{q} - \frac{\gamma\tau}{q^2}\right) & 1 + 2\left(\frac{\tau}{q} - \frac{\gamma}{q} - \frac{\gamma\tau}{q^2}\right) \end{pmatrix} \tag{50}$$

The betatron stability condition is

$$Tr(\bar{M}_{TCT}) = 2(1 + 2(\frac{\tau}{q} - \frac{\gamma}{q} - \frac{\gamma\tau}{q^2}) \leq 2 \tag{51}$$

If one takes $\gamma=q$, i.e. $qC=L$ as above, then the equality holds in eq. 51 regardless of τ. Thus, the system is on the borderline of strict stability so that one is justified in cascading several such cells.

It has been noted that β_T, the primary beam beta-function in the target, is the maximum value of β. One would like to make this small as possible. Employing the same variables in eq. 45 one finds

$$\beta_T = L\sqrt{\frac{1 + \gamma}{(1-\tau)(\tau-\gamma+\gamma\tau)}} = \frac{L}{\sin \mu/2}\sqrt{\frac{1 + \gamma}{1 - \tau}} \tag{52}$$

The minimum $\beta_T=0$ occurs for $\gamma=q$; the minimum attainable β_T under this condition occurs for

$$\tau_{opt} = \frac{1 + 2q}{2(1+q)} \cdot \tag{53}$$

Substituting this value of τ into eq. 44 along with $\gamma=q$ shows that

the phase advance for minimum β_T is

$$\frac{\mu_{opt}}{2} = \sin^{-1} \sqrt{\tau_{opt} - q + q\tau_{opt}} = \sin^{-1}(1/2) = \pi/6 \tag{54}$$

so that

$$\beta_{Topt} = \frac{L}{\sin \mu_{opt}/2} \sqrt{\frac{1+q}{1-\tau_{opt}}} = 2L(1+q) \backsim 2L \tag{55}$$

Thus, the smallest beam spot one can obtain is determined by β somewhat larger than the cell length.

The trouble with these rather tidy looking results is that the ansatz $\gamma=q$ applies to $\bar{\beta}_T \equiv 0$; eq. 39 however, states that proper matching requires a generally small, but unequivocally non-zero, $\bar{\beta}_T$. Therefore, parameters determined from eqns. 40-55 are only approximate starting values for a somewhat less straightforward search. The procedure which has been used in finding thick lens solutions is to start with values from the thin lens calculation and solve equation 37 for β_T and its analog for $\bar{\beta}_T$ simultaneously by numerical means to give the required currents in target and collector. The solution is repeated for a set of plausible target and collector lengths to allow the selection of a solution

combining the shortest collector length having tolerable current with a target having acceptable current and length near optimum for depth of field. A bit of trial and error is required because, with γ no longer rigidly fixed at q and with the system always near the border of the stable region for the secondary beam, it is easy to get divergent solutions while adjusting β's.

VI.
Monte Carlo Calculations of Secondary Beam Phase Space Distribution

The discussion in the preceding three sections employs purely conventional linear beam optics which take no account of the repulsive potential, the λ-term in eq. 7, affecting particles not coplanar with the lens axis. In order to get beam profiles corresponding to non-zero emittances some sort of ray tracing is required. Besides wanting to demonstrate that the neglect of that term is justified, one would like to see how the emittance of particles produced throughout the target looks in the focal plane of some collection system, including not only the beam optics but presumably multiple coulomb and nuclear scattering as well. The examples presented in the next section were calculated by using a program which starts from a primary beam with a cylindrically symmetric gaussian distribution of transverse coordinates and momenta. The distribution is generated at a waist and then transformed to a correctly matched distribution at the upstream end of the target by choosing a suitable β-function at the waist and drift distance from the waist. Multiple coulomb scattering of

the primary beam is calculated according to the standard Rossi formula[13] with thin target correction as needed, and nuclear scattering is calculated according to the parameterization of Bellitini et al.[14] in a Monte Carlo with step size small enough so that the effect of magnetic field on the trajectory can be adequately represented by an angle kick and the inelastic interaction probability per step is small[15]. When an inelastic interaction occurs it is treated as the production of a secondary within the longitudinal momentum bite of interest with gaussian angular distribution characterized by an rms transverse momentum $<\bar{p}_\perp>$

$$\bar{\theta}_{rms} = <\bar{p}_\perp>/\bar{p} \ . \tag{56}$$

The secondary particles are followed along with the remaining primaries with appropriate values for the absorption length etc. To convert Monte Carlo yields to absolute yields one must normalize by the ratio of foward production cross section into the given momentum bite to the total inelastic cross section.

In the following section this Monte Carlo program is applied to antiproton production using the targeting schemes discussed in sections II-V. The parameters are given in Table I. Although these do not apply precisely to any existing or planned facility they may serve as well as any to give concrete illustration of the

foregoing conceptual development and to suggest wherein realistic cases may differ from the simplifications used. The absolute yield figures quoted are intended to be indicative only. The major emphasis has been on comparison of relative yield which is largely insensitive to assumptions about the details of the production. Thus, simple assumptions have been made which may result in as much as a factor of two error in the total production. For instance, the A-dependence of the forward production cross section is assumed to be the same as the A-dependence of the total inelastic cross section and $<\vec{p}>$ is assumed independent of A. For more realistic treatment of the absolute production of antiprotons one needs a careful treatment of the scanty experimental data[16]. The examples differ somewhat in the completeness of the optimization, but the attempt was made to at least ascertain the ranking of the various schemes for the chosen application. Although engineering feasibility is not addressed, an effort is made to observe plausible limits on properties of materials, etc.

Table I

Parameters for Antiproton Production by Protons

Employed in Illustrative Examples

p	proton momentum	80 GeV/c
$\bar{p}$	antiproton momentum	5.4 GeV/c
$\Delta\bar{p}_{\parallel}$	antiproton momentum bite (full width)	4%
ϵ	proton rms emittance	20 π mm-mrad
$\bar{\epsilon}$	antiproton beam full acceptance	.05 π mm-mrad
β	minimum Courant-Snyder beta for proton beam	1 m
$\lambda=\bar{\lambda}$	absorption length (taken as same for proton & antiproton)*	
	Li	120.6 cm
	Be	36.7 cm
	W	10.3 cm
X_o	radiation length†	
	Li	155 cm
	Be	35.3 cm
	W	.35 cm
B_{max}	maximum allowed value of surface magnetic field	
	Li•	180 kG
	Be§	180 kG
$\langle\bar{p}_{\perp}\rangle$	rms transverse momentum of antiprotons§§	.325 GeV/c
$(E\frac{d^3\sigma}{dp^3})_{p_{\perp}=0}$	invariant forward production cross section§§§	.8 mb GeV^{-2}

Notes *Absorption lengths from "Particle Properties Data Booklet", abstracted from RMP, 52 , (April 1980). The approximation $\lambda=\bar{\lambda}$ is reasonably good for lithium and beryllium, not so good for tungsten.

†"Particle Properties Data Booklet", sup. cit.

*T.A. Vsevolozhskaya et al., ZhTF, XLV (1975), p. 2494

§Author's guess - depends on alloy and/or crystalization properties.

§§The angular distribution is somewhat broader for $\bar{p}$ than for pi's; this approximate $\langle \bar{p}_\perp \rangle$ figure reflects that qualitative observation but is not the result of detailed fits to the data.

§§§J.W. Cronin, 1977 Fermilab Summer Study, V. 1, p. 269.

VII. Specific Examples

Although each of these targeting strategies has been examined in some detail, no conclusion has been offered about relative performance. Clearly simplicity favors the single current carrying target; it seems that only rather special circumstances could justify so elaborate a scheme as a multicell alternating gradient channel. This section treats in a more concrete way a comparison of the three schemes for the specific application of 5.4 GeV/c antiproton production by 80 GeV/c protons; the complete specification of the application is embodied in Table I. For each scheme an initial design was chosen according to the principles discussed in Sections III-V and a sufficient number of Monte Carlo calculations were made to give parameters optimizing yield to within about 10%. Several non-optimum cases are also reported to illustrate parametric dependences. Table II displays the relative yield for the various cases normalized to that of a 5.7 cm tungsten target. These relative yields are a measure of the optical efficiency of the schemes. The column for absolute production is based on 2×10^{12} protons for the tungsten target and 8×10^{12} for beryllium. These primary beam intensities are based on results of the nuclear cascade Monte Carlo CASSIM for energy deposition[17] and the thermal properties of the metals[18] assuming an instantaneous beam spill. The principal parameters of the targeting systems are included in Table II also; the details are covered in the following text. Although the qualitative features of this comparison surely hold for similar cases, there may be

different conclusions appropriate for very different applications.

A. Current Carrying Target

The value of the required surface magnetic field does not permit satisfying eqn. 14 for the full 60 mrad corresponding to $\langle \bar{p}_\perp \rangle = .325$ GeV/c. By backing off to 25 mrad a useable solution is obtained, but this represents a major retreat from the ideal case. If there is some beryllium alloy able to take stronger current pulses, a better angular acceptance could be obtained, but the limit set by defocusing of primary beam also restricts k for the given primary momentum to somewhat less than required to satisfy eqn. 14, viz $\bar{k}=\pi\ \bar{\theta}^2_{max}/\bar{\varepsilon}=180\ m^{-1}$. Applying the limiting criterion o@G one obtains $\bar{k} < 164\ m^{-1}$. Thus, if the target could stand the strain one would probably take $\bar{k}\backsim 50\pi$ instead of the 10π used in this example. Figure 4 shows x-x′ scatter plot of the secondary beam at the end of the target. The 20π mm-mrad acceptance ellipse is indicated by the asterisks in Figure 4A and the actual number of particles represented by each asterisk is plotted separately in Figure 4B. There are 9270 antiproton points plotted of which 5018 lie within the acceptance. Figure 4C gives the x-x′ distribution of the 60K of the original 100K primary protons which fail to interact; 8K of the survivors are outside the angular range of the plot. One notes that the gradient and target radius have been chosen so that nearly all of the proton beam is within the target radius at the ends. The absence of antiprotons with x>.0012 m comes from a program limit introduced to save time by not following particles far outside of the final acceptance.

Besides the solution for $\bar{k}L=2\pi$ solutions for 0, π and $\sim 4\pi$ are included. The k=0 solution gives a reference value for the kind of gains which can be obtained for this case. The $\bar{k}L=4\pi$ case was included to show that the optimum target length is substantially less than the absorption length λ indicated by the discussion of eq. 10. In this case $\bar{k}$ was held fixed and L was set equal to λ. The length optimization was not carried through many iterations, but it is worth mentioning that whatever the optimum obtained by the methods used here, the development of the nuclear cascade means that the true optimum is somewhat longer. The $\bar{k}L=\pi$ solution is the one corresponding to Figure 1, but as the relation (eq. 14) between acceptance and $\bar{k}$ shows, too much acceptance is lost to beam width in this case.

B. Multiple Targets

The multiple target comparison has been made holding total target length to the $\sim$20 cm value which was optimum in the current carrying target case. The point primarily is to demonstrate what fraction of the efficiency of that arrangement could be retained with lumped focusing. This alternative is attractive for a case where the optimum material for production use is unsuitable as a lens because of conductivity, mechanical properties, or the like. The results are included in Table II tell most of the story. The collection lenses were matched to the 36.5 mrad angle implied by the given primary beam ϵ and β by

$$\bar{\theta}_{max} = \bar{\epsilon}/\sqrt{6\epsilon\beta} \qquad (57)$$

where the full acceptance is $\bar{\epsilon}$ and ϵ is the rms primary beam emittance. For these collection lenses the target waist has β_T=.015 so that one would expect some gain in dividing the target down to ∿3 cm lengths were it not for losses in the intervening lenses.

Figure 5 contains x-x′ distributions of the antiprotons and protons at the target array in the same form as Figure 4 for the optimized current carrying target.

C. Alternating Gradient Target Channel

The strategy of interleaving targets focusing for the primary beam with axially focusing lenses for the secondaries has the conceptual appeal of dealing with the depth of field question simultaneously for both beams so that it would appear that the compromises required in the other two techniques are avoided. Unfortunately, the compromises are merely recast; the primary beam has to be at its widest in the production target where one would of course like the smallest possible beam width. Thus, the design question is whether the optimized target channel adapts to the necessary compromises better than the other schemes. The results shown in Table II show that for the present case the answer is clearly negative. On the other hand, primary beam depth-of-field could be a much more important problem in a case where the ratio of secondary to primary momentum is closer to one. The target channel results given in Table II all refer to the same basic solution; the several entries refer to different numbers of the

same cell. See Figure 6 for the beam distributions. Despite its poor relative showing in this illustrative example the axially focusing alternating gradient target channel may have an appropriate application. Calculations for a small acceptance case show the channel having a higher yield than a tungsten target[6].

Attempts to push the alternating gradient scheme to greater efficiency in this application have not been successful. The reasoning outlined in Sec. V leads to a conclusion that the antiproton beta function at the target waist should be $\bar{\beta}_T$=.015 just as in the multiple target array case. However, although it is perfectly possible to get parameters for an apparently analogous solution with that $\bar{\beta}_T$,the alternating gradient array does not perform as well. By lengthening the cell by ∿16% and doubling $\bar{\beta}_T$ as given in Table II the performance is improved slightly, but not above the level attained by either of the other techniques. This failure of the linear optics design strategy to give a reasonable approximation to optimum parameters illustrates the cautionary note expressed in Sec. II; the linear optics treatment properly applies only to a zero emittance sample of the primary and secondary beams and any plausible conclusions arising from it must be tested by some more complete technique such as the Monte Carlo which has been used.

D. Summary

Of the techniques discussed for improving the collection efficiency for secondaries from a long target, the current carrying or self-focusing target is not only the most

straightforward but also the most effective in the illustrative example. It was suggested that special circumstances could favor more elaborate schemes. The multiple short target array with the focusing provided by interleaved lithium lenses was presented as a possible solution for cases in which the optimum target material has poor properties for acting as a pulsed lens as well. Both of these schemes give Monte Carlo yield results reasonably in accord with the linear optics approximations which have been developed and have apparent advantage over a shorter tungsten target in the $\bar{p}$ production example. The extension of the optical analysis to a yet more elaborate arrangement providing alternating sign of the focusing to provide increased depth-of-field for both primary and secondary beams does not appear to give such a useful guide to optimum parameters. In the absence of a more sophisticated analytical treatment a Monte Carlo approach like the one described here can be used to explore the effectiveness of the scheme for novel conditions.

The beam optics of a conductor carrying uniform current density has been exploited in three variants to improve the collection of secondaries from a long target. Although compromises are necessary to accommodate the properties of real materials, the defocusing of the primary beam, etc. it is possible to attain a collection efficiency competitive with much shorter conventional targets. What little has been lost in efficiency is made up several fold in production capability because of the superior primary beam tolerance of low-Z material.

REFERENCES

1. G. Bohannon, "Target Behavior Calculations" in Proceedings of High Intensity Targeting Workshop, Fermilab (4/28-4/30/80), D. Cline, U. Wisc., organizer.

2. The term "current monopole lens" to describe axial current focusing devices in general appears in T.B.W. Kirk, "$\bar{p}$ Production Target Studies-Numerical Calculations", Fermilab unpublished TM-1011 (11/14/80). The designation is apt and should probably be perpetuated.

3. This idea was suggested by G.I. Budker in 1976 according to L.N. Blumberg and A.E. Webster, "Secondary Yield Enhancement from Current Carrying Target", IEEE Trans. on Nucl. Sci., v. NS-24, #3, p. 1539 (6/77).

4. Lithium lenses developed at Inst. for Nuclear Physics, Novosibirsk, are described in T. Vsevolozhskaya et al., "Optical Properties of Cylindrical Lenses", Soviet Technical Physics (AIP Translation), V20, #12 (12/75).

5. G.I. Budker et al., Proc. V Sov. Nat'l Conf on Part Acc., v. II, p. 299, Dubna (1976).

6. J.A. MacLachlan et al., "Pulsed High Current Optics for $\bar{p}$ Production at 5.4 GeV/c", IEEE Trans. on Nucl. Sci., v. NS-28, #3, p. 2785 (6/81).

7. Design Report Tevatron Phase I Project, Fermilab (2/80).

8. The Fermilab Antiproton Source Design Report, Fermilab (2/82).

9. The enthalpy reserve between 20°C and the melting point is ~500 J/gm for W and 3000 J/g for Be. Priv. comm., C. Canada (1981).

10. This "obit Lagrangian" formalism for the trajectories has been borrowed from L.C. Teng.

11. B.F. Bayanov and G.I. Silvestrov, "Soviet Technical Physics (AIP Translation), v. 48, #1", (1978).

12. B.F. Bayanov et al., "A Lithium Lens for Axially Symmetric Focusing of High Energy Particle Beams", Nucl. Inst. and Meth., v. 190, p. 9, (1981).

REFERENCES (continued)

13. E. Segre, Experimental Nuclear Physics, John Waley and Sons, New York, p. 285 (1953).

14. G. Bellettini et al., Nucl. Phys. 79, p. 609 (1966).

15. J. MacLachlan et al., "Monaco, a Monte Carlo Trajectory Fortran IV Subroutine for High Energy Protons in Bulk Material", Fermilab unpublished TM-244 (May, 1970).

16. C. Hojvat and A. Van Ginneken, "Calculation of Antiproton Yields for the Fermilab Antiproton Source", Fermilab-Pub-82/43, (submitted to Nucl. Inst. & Meth) (July, 1982).

17. A. Van Ginneken, Fermilab FN-272 (1975).

18. Values from standard sources provided by C. Canada, private communication.

FIGURE CAPTIONS

Figure 1: Production target with axial focusing.

Figure 2: Multiple target array.

Figure 3: Axially focusing alternating gradient target channel.

Figure 4: Projection of $\bar{p}$ phase space on x-x′ plane at end of current carrying target.

(a) all $\bar{p}$
(b) accepted $\bar{p}$
(c) non-interacting protons

Figure 5: Projection of $\bar{p}$ phase space on x-x′ plane at end of 3 cell segmented target array.

(a) all $\bar{p}$
(b) accepted $\bar{p}$

Figure 6: Projection of $\bar{p}$ phase space on x-x′ plane at end of 3 cell alternating gradient target channel

(a) all $\bar{p}$
(b) accepted $\bar{p}$

Figure 7: Projection of $\bar{p}$ phase space on x-x′ plane at end of 5.5 cm W target, reference case.

(a) all $\bar{p}$
(b) accepted $\bar{p}$
(c) non-interacting protons

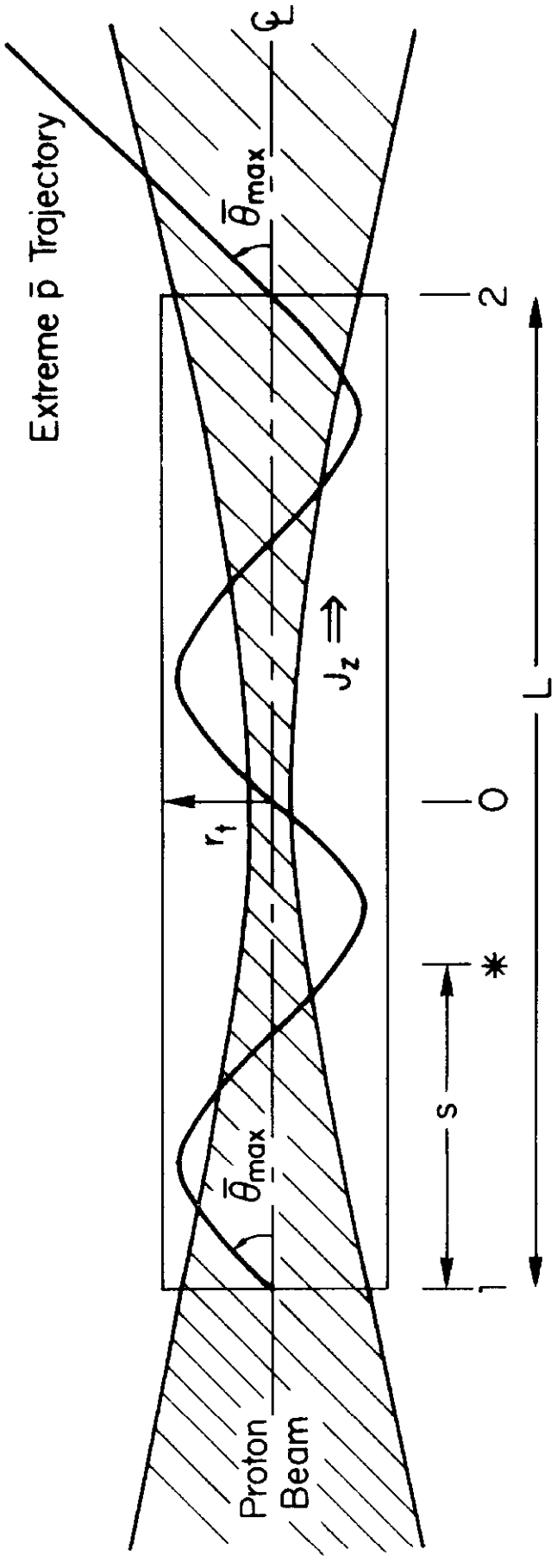

Figure 1: Axially Focusing Target

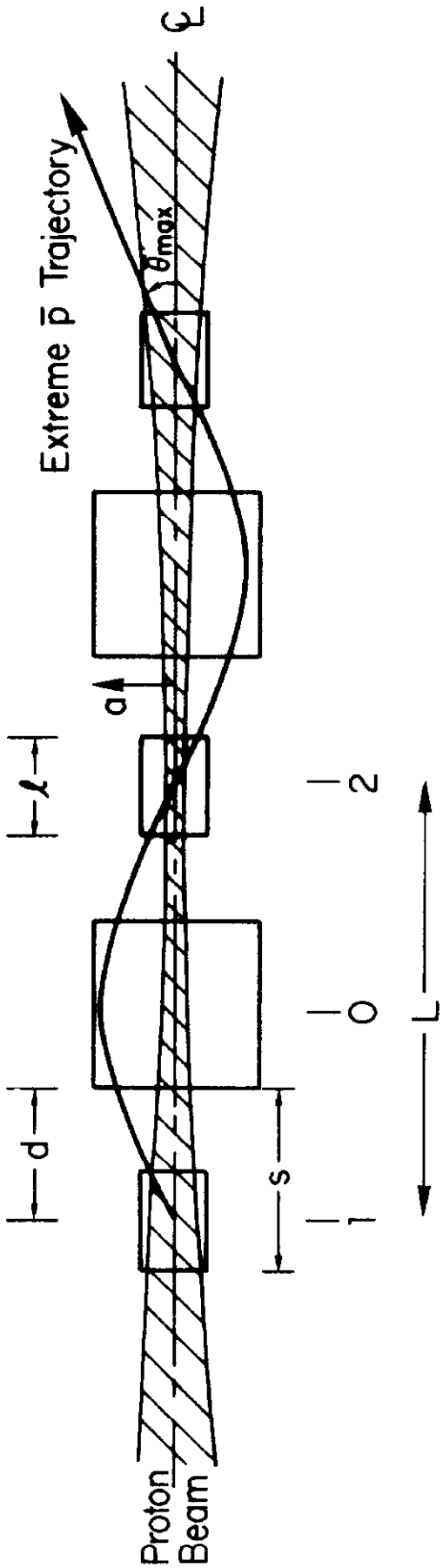

Figure 2: Multiple Target Array

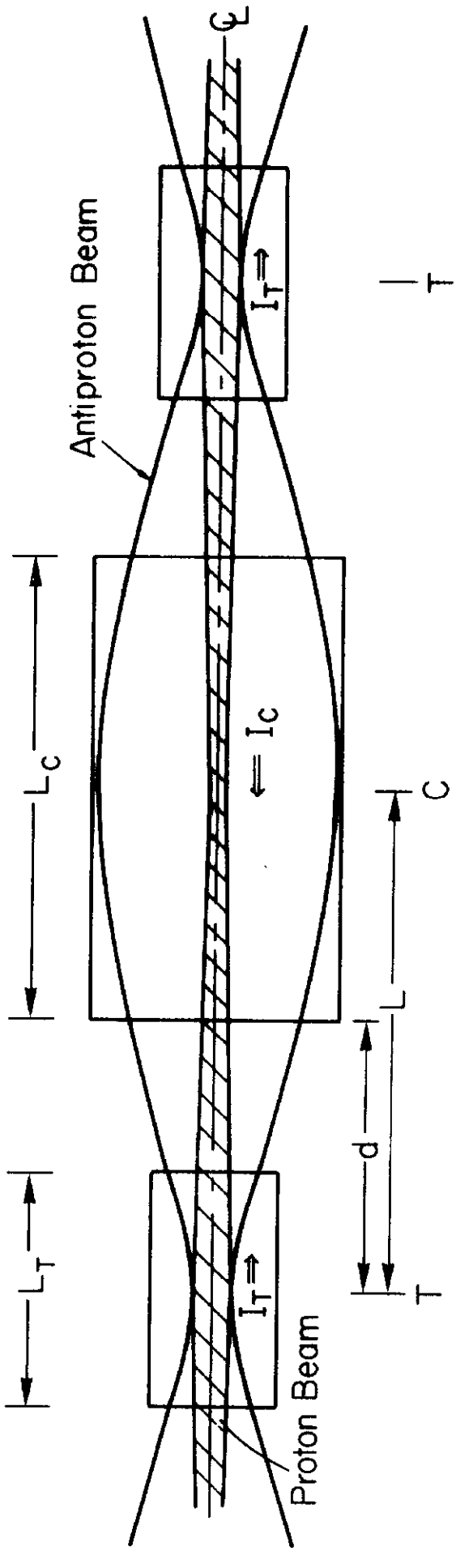

Figure 3: One Cell of Alternating Gradient Target Channel

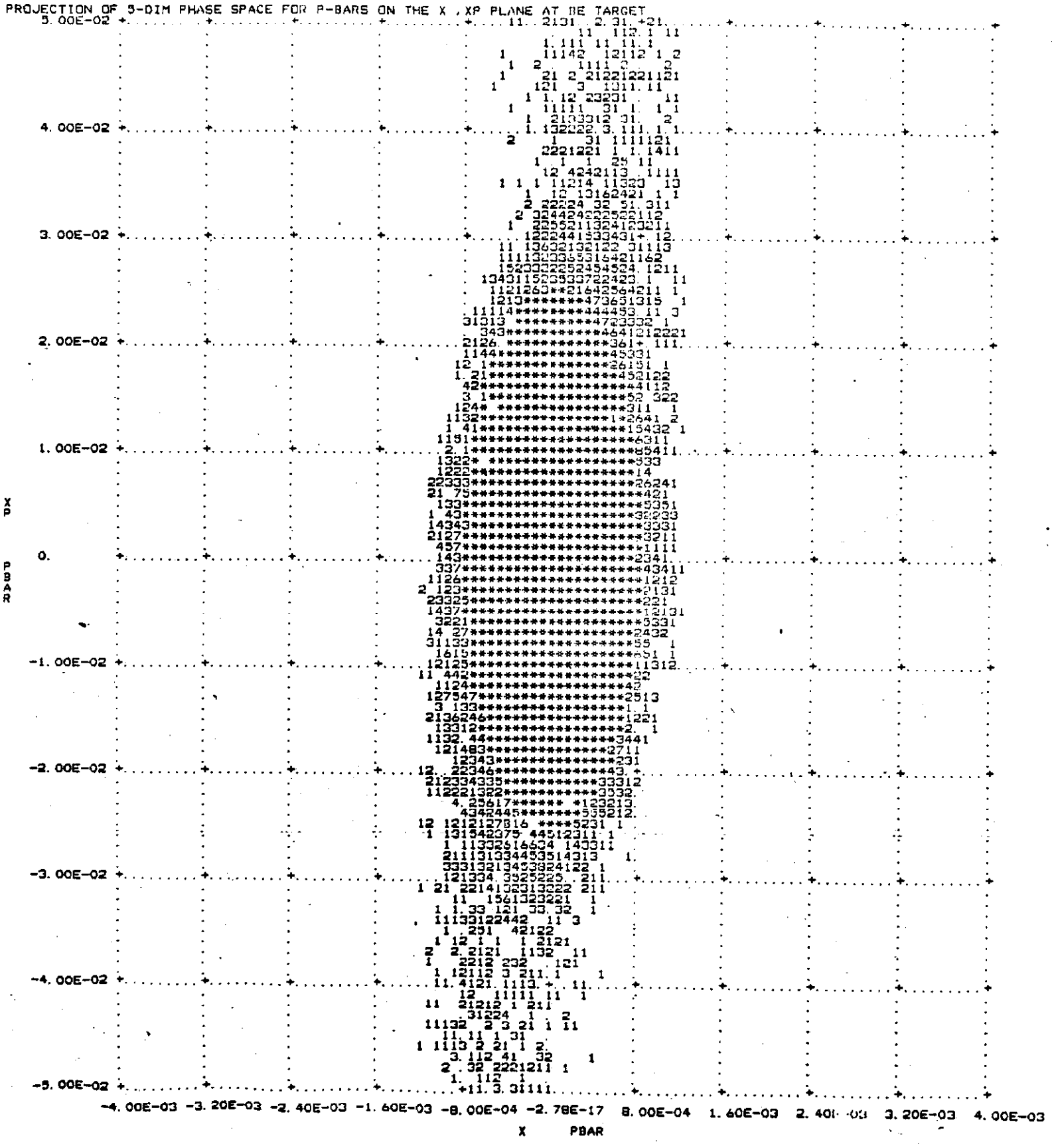
PROJECTION OF 5-DIM PHASE SPACE FOR P-BARS ON THE X , XP PLANE AT BE TARGET
5.00E-02
4.00E-02
3.00E-02
2.00E-02
1.00E-02
0.
-1.00E-02
-2.00E-02
-3.00E-02
-4.00E-02
-5.00E-02
XP
PBAR
-4.00E-03 -3.20E-03 -2.40E-03 -1.60E-03 -8.00E-04 -2.78E-17 8.00E-04 1.60E-03 2.40E-03 3.20E-03 4.00E-03
X PBAR

Fig. 4a

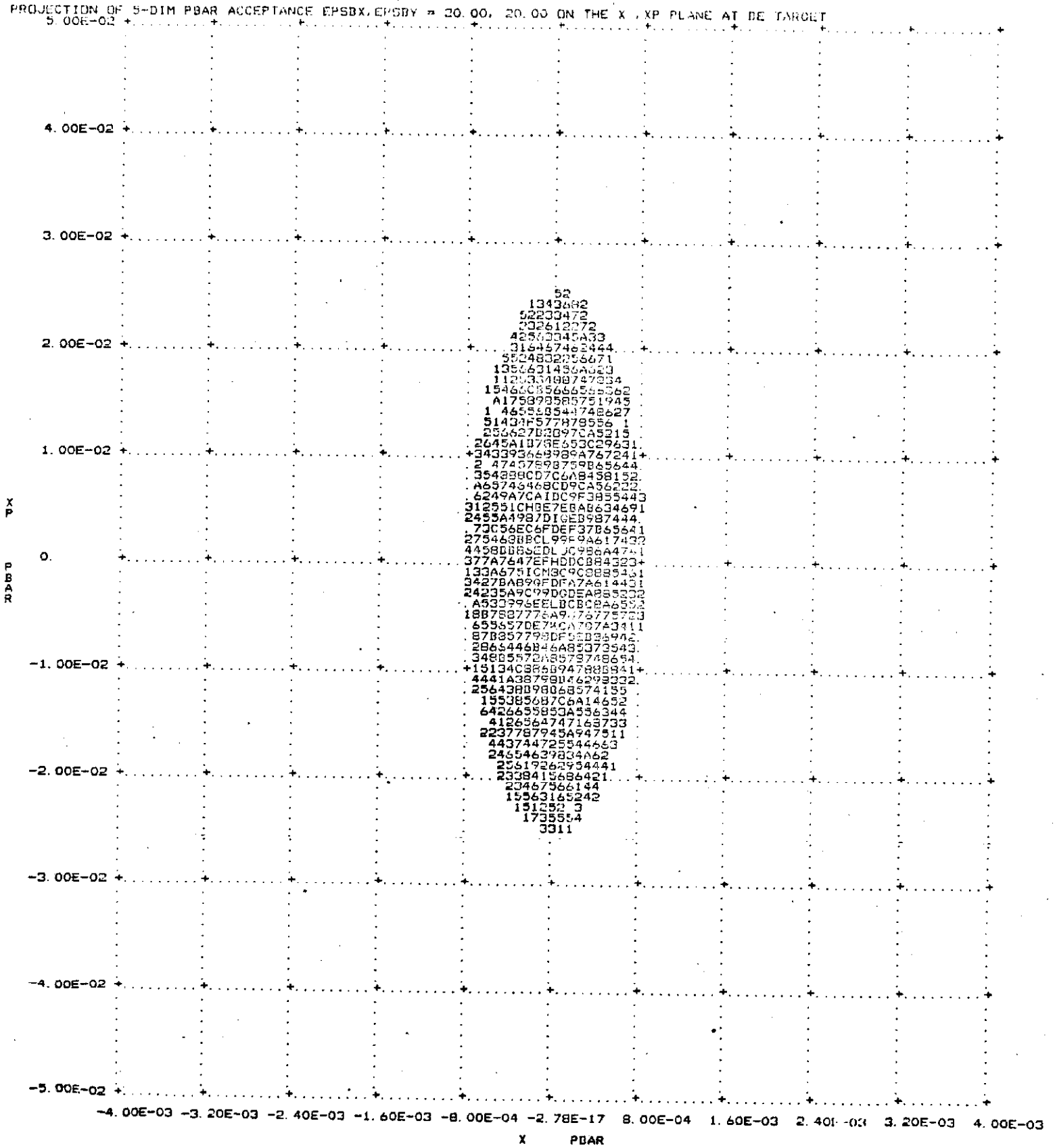
PROJECTION OF 5-DIM PBAR ACCEPTANCE EPSBX,EPSBY = 20.00, 20.00 ON THE X , XP PLANE AT BE TARGET
5.00E-02
4.00E-02
3.00E-02
2.00E-02
1.00E-02
0.
-1.00E-02
-2.00E-02
-3.00E-02
-4.00E-02
-5.00E-02
XP
PBAR
-4.00E-03 -3.20E-03 -2.40E-03 -1.60E-03 -8.00E-04 -2.78E-17 8.00E-04 1.60E-03 2.40E-03 3.20E-03 4.00E-03
X PBAR

Fig. 4b

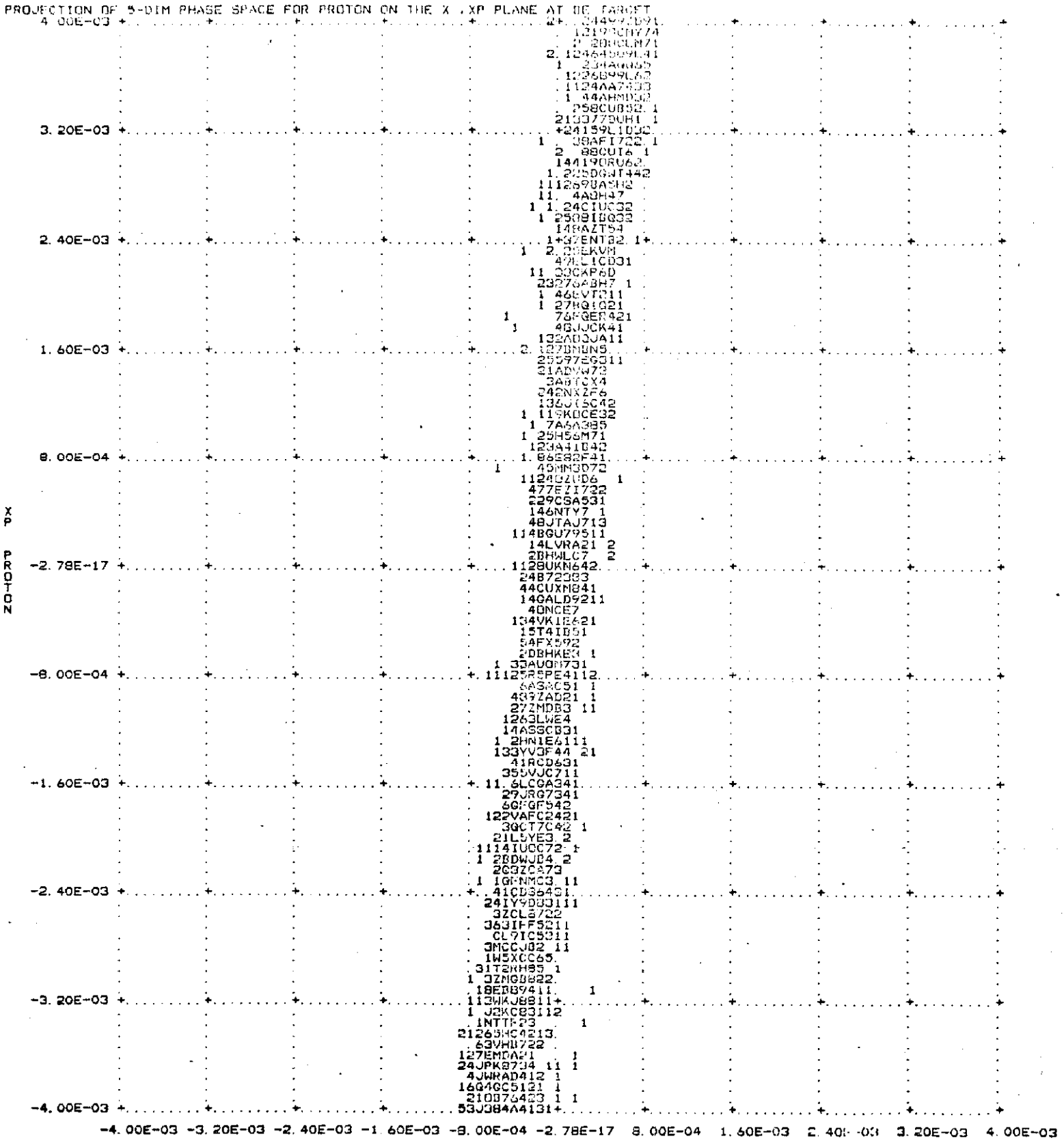
PROJECTION OF 5-DIM PHASE SPACE FOR PROTON ON THE X ,XP PLANE AT DE TARGET
4.00E-03
3.20E-03
2.40E-03
1.60E-03
8.00E-04
-2.78E-17
-8.00E-04
-1.60E-03
-2.40E-03
-3.20E-03
-4.00E-03
XP PROTON
-4.00E-03 -3.20E-03 -2.40E-03 -1.60E-03 -8.00E-04 -2.78E-17 8.00E-04 1.60E-03 2.40E-03 3.20E-03 4.00E-03

Fig. 4c

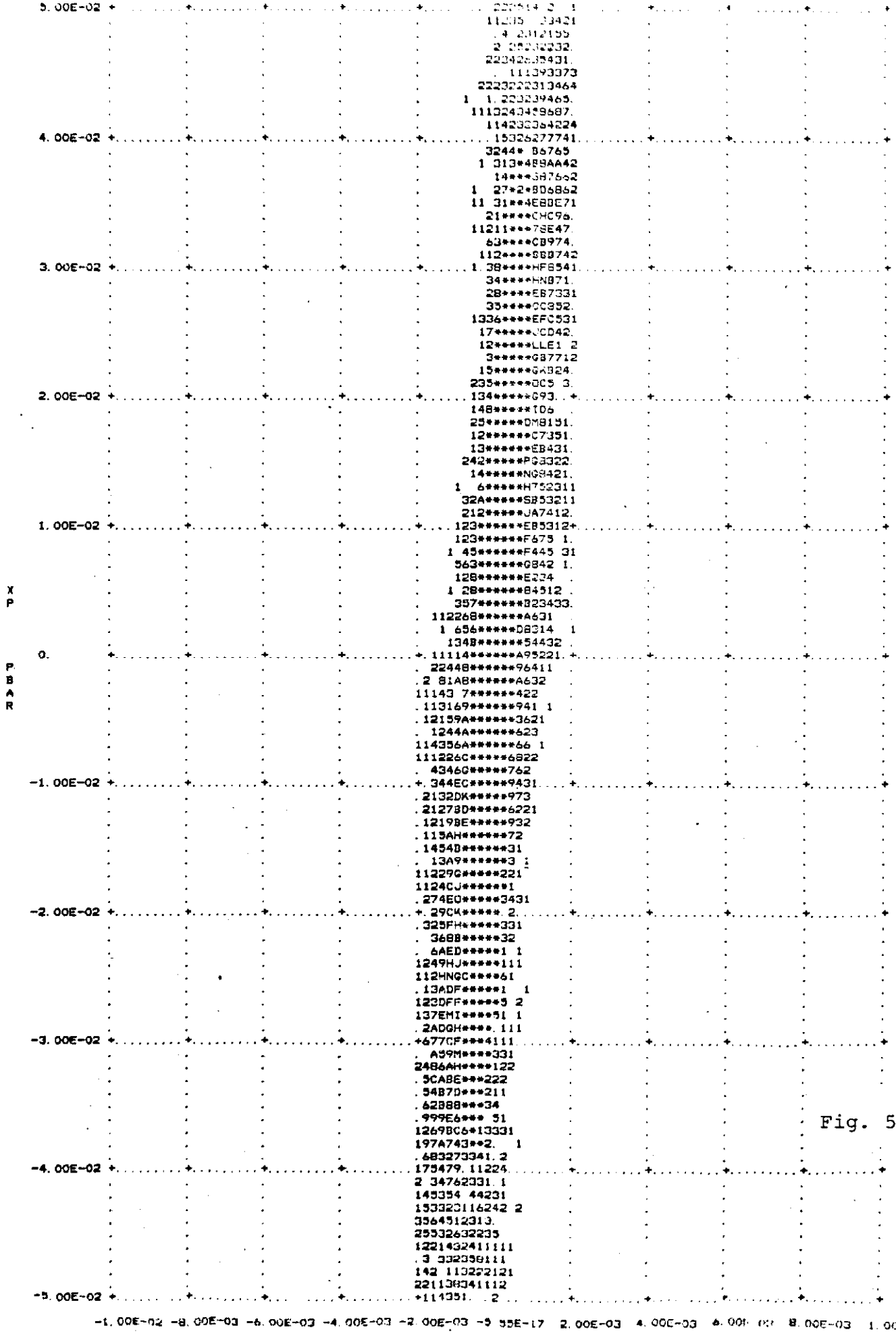
PROJECTION OF 5-DIM PHASE SPACE FOR P-BARS ON THE X , XP PLANE AT DL TOT 3
5.00E-02
4.00E-02
3.00E-02
2.00E-02
1.00E-02
0.
-1.00E-02
-2.00E-02
-3.00E-02
-4.00E-02
-5.00E-02
XP
PBAR
-1.00E-02 -8.00E-03 -6.00E-03 -4.00E-03 -2.00E-03 -5.55E-17 2.00E-03 4.00E-03 6.00E-03 8.00E-03 1.00E-02
X PBAR

Fig. 5a

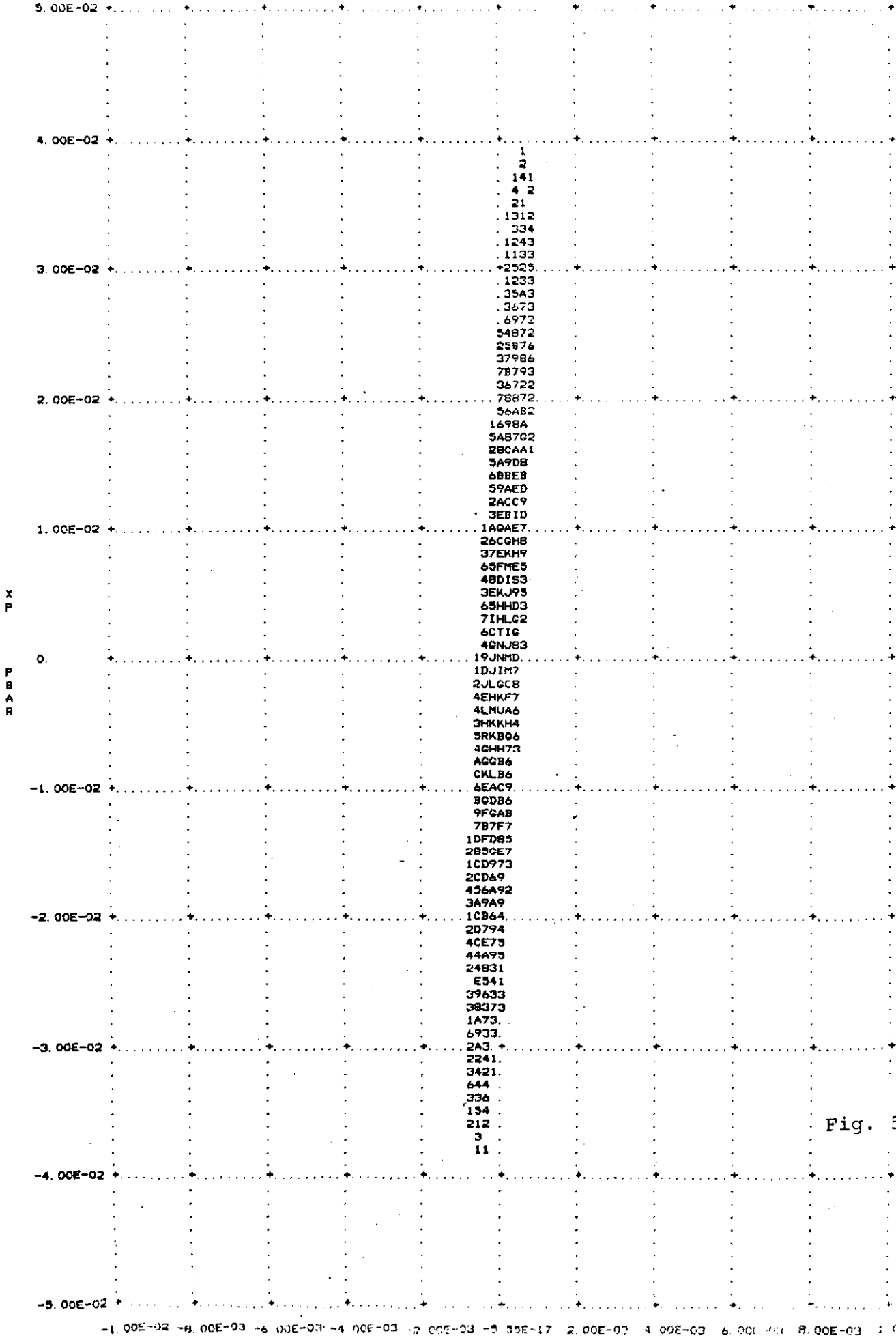
PROJECTION OF 5-DIM PBAR ACCEPTANCE EPSBX,EPSBY = 20.00, 20.00 ON THE X ,XP PLANE AT BE TGT 3
5.00E-02
4.00E-02
3.00E-02
2.00E-02
1.00E-02
0.
-1.00E-02
-2.00E-02
-3.00E-02
-4.00E-02
-5.00E-02
XP
PBAR
-1.00E-02 -8.00E-03 -6.00E-03 -4.00E-03 -2.00E-03 -5.55E-17 2.00E-03 4.00E-03 6.00E-03 8.00E-03 1.00E-02

Fig. 5b

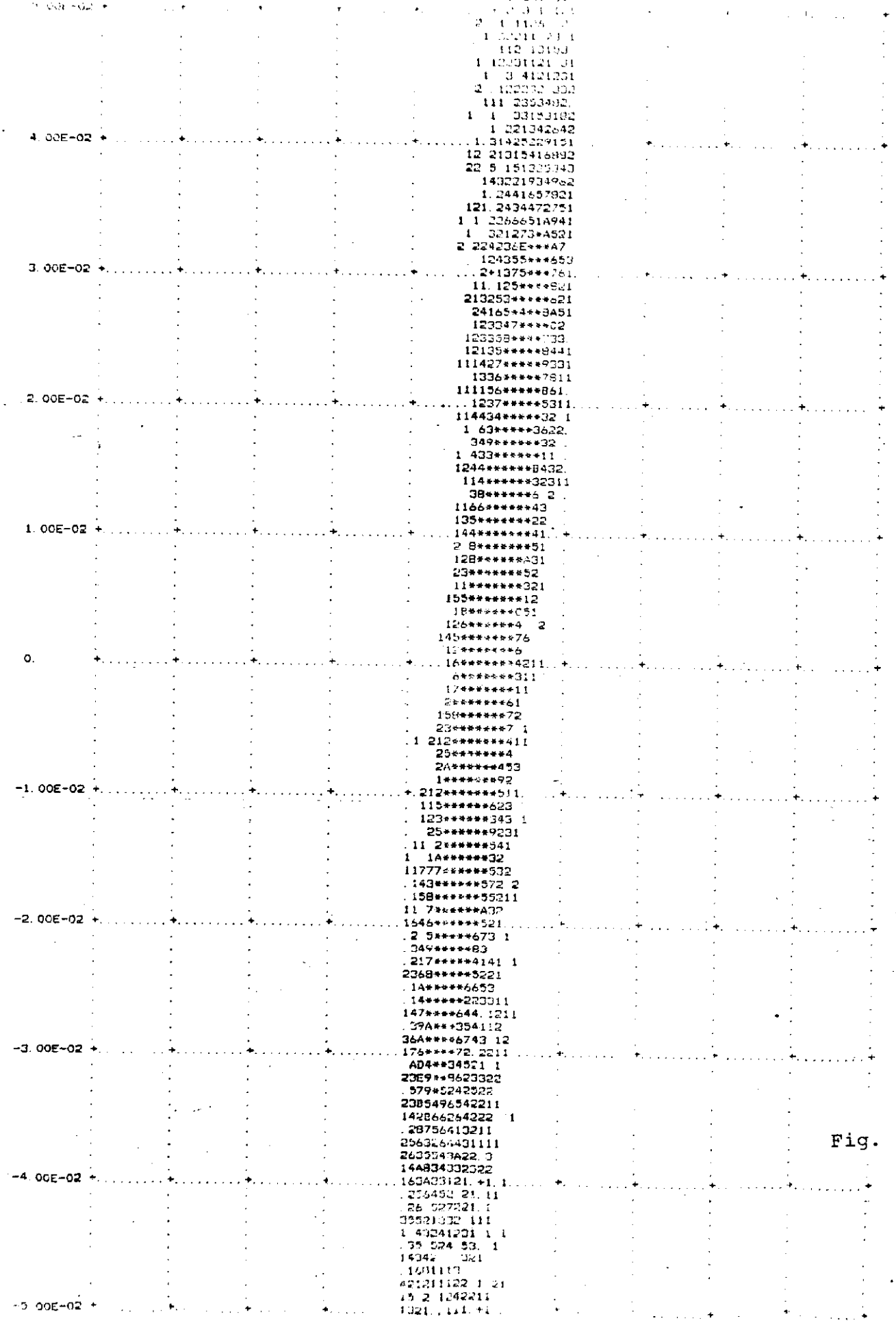
4.00E-02
3.00E-02
2.00E-02
1.00E-02
0.
-1.00E-02
-2.00E-02
-3.00E-02
-4.00E-02
-5.00E-02

Fig. 6a

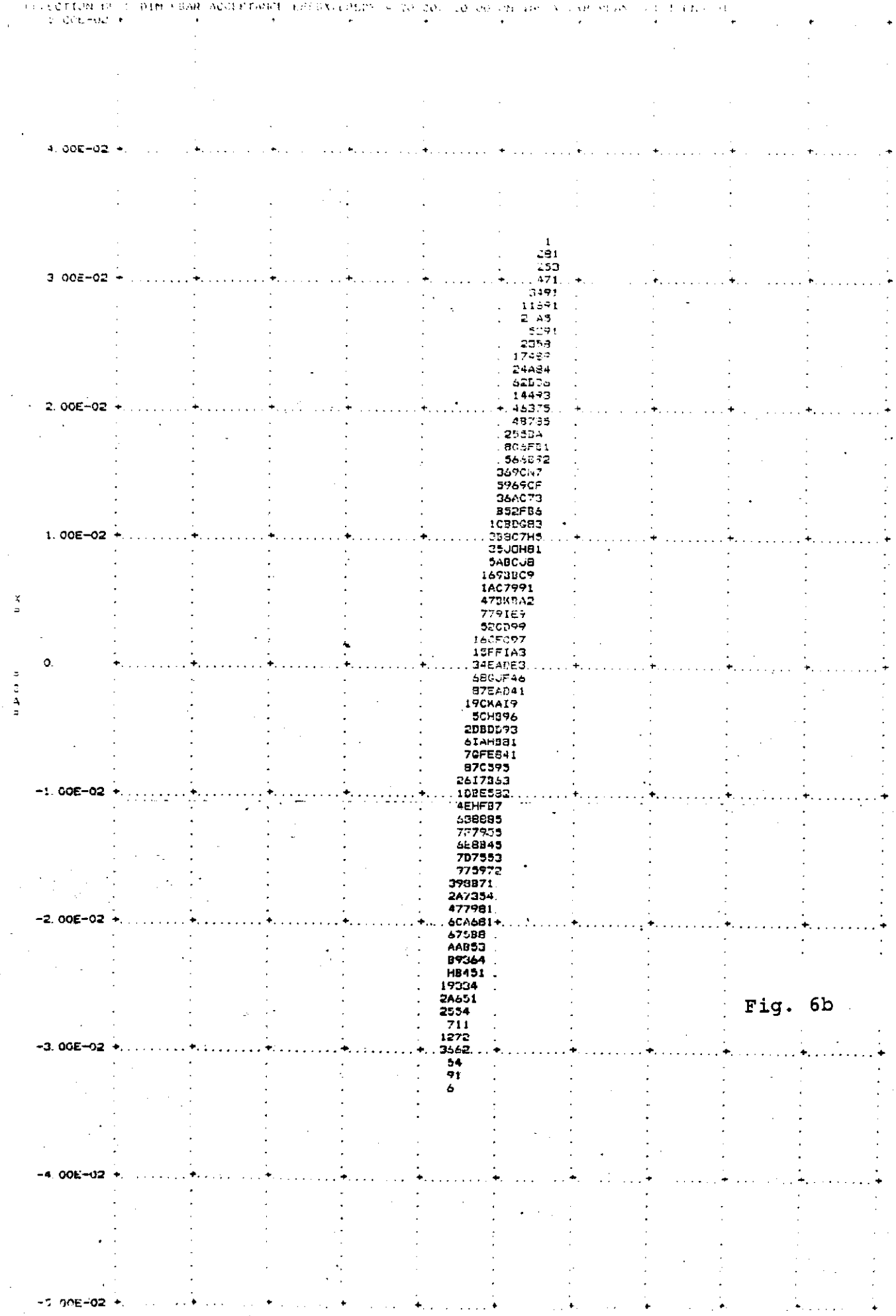
4.00E-02
3.00E-02
2.00E-02
1.00E-02
0.
-1.00E-02
-2.00E-02
-3.00E-02
-4.00E-02
-5.00E-02
-1.00E-02 -8.00E-03 -6.00E-03 -4.00E-03 -2.00E-03 0. 2.00E-03 4.00E-03 6.00E-03 8.00E-03 1.00E-02

Fig. 6b

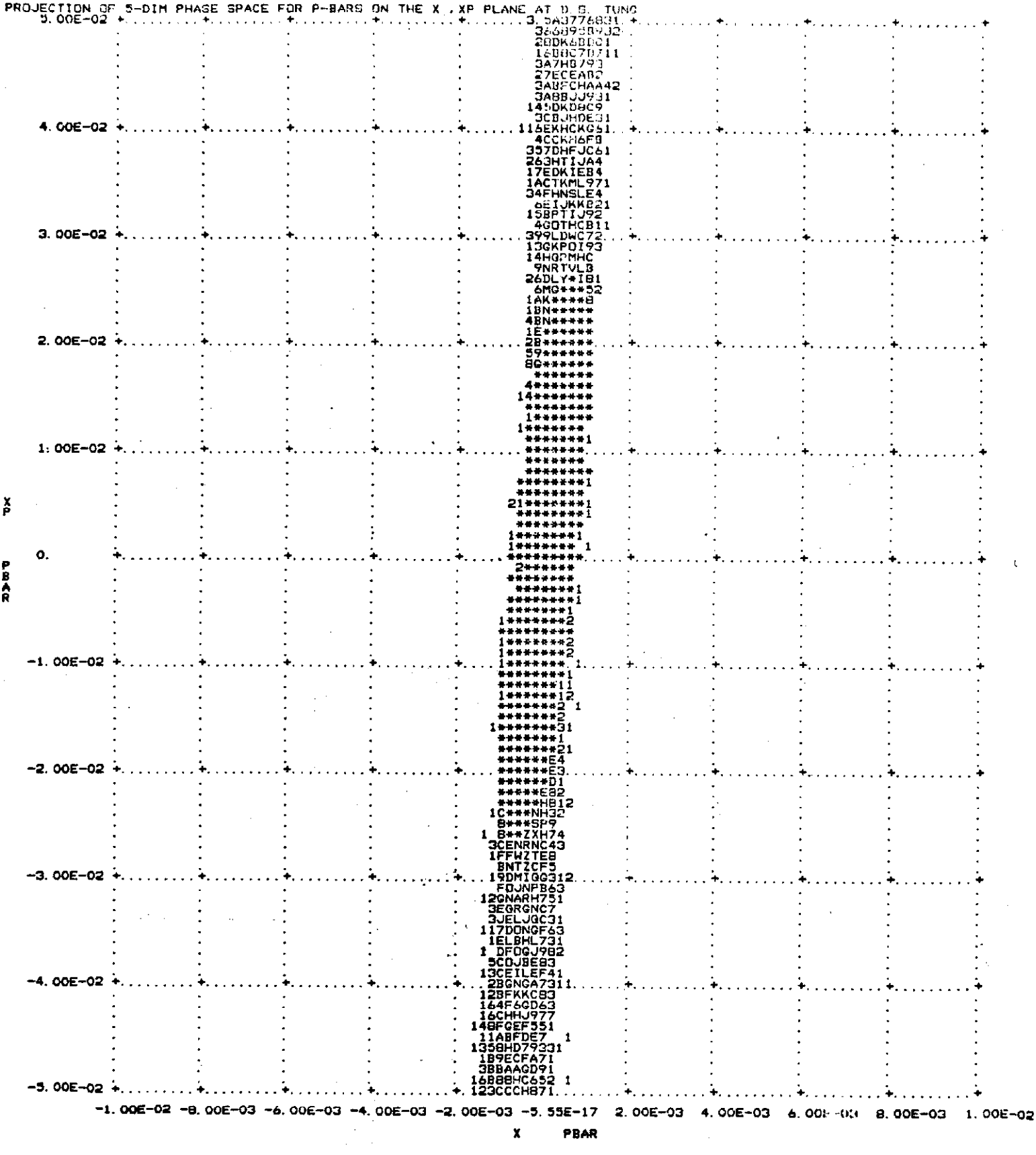
PROJECTION OF 5-DIM PHASE SPACE FOR P-BARS ON THE X , XP PLANE AT D.S. TUNE
5.00E-02
4.00E-02
3.00E-02
2.00E-02
1.00E-02
0.
-1.00E-02
-2.00E-02
-3.00E-02
-4.00E-02
-5.00E-02
XP PBAR
-1.00E-02 -8.00E-03 -6.00E-03 -4.00E-03 -2.00E-03 -5.55E-17 2.00E-03 4.00E-03 6.00E-03 8.00E-03 1.00E-02
X PBAR

Fig. 7a

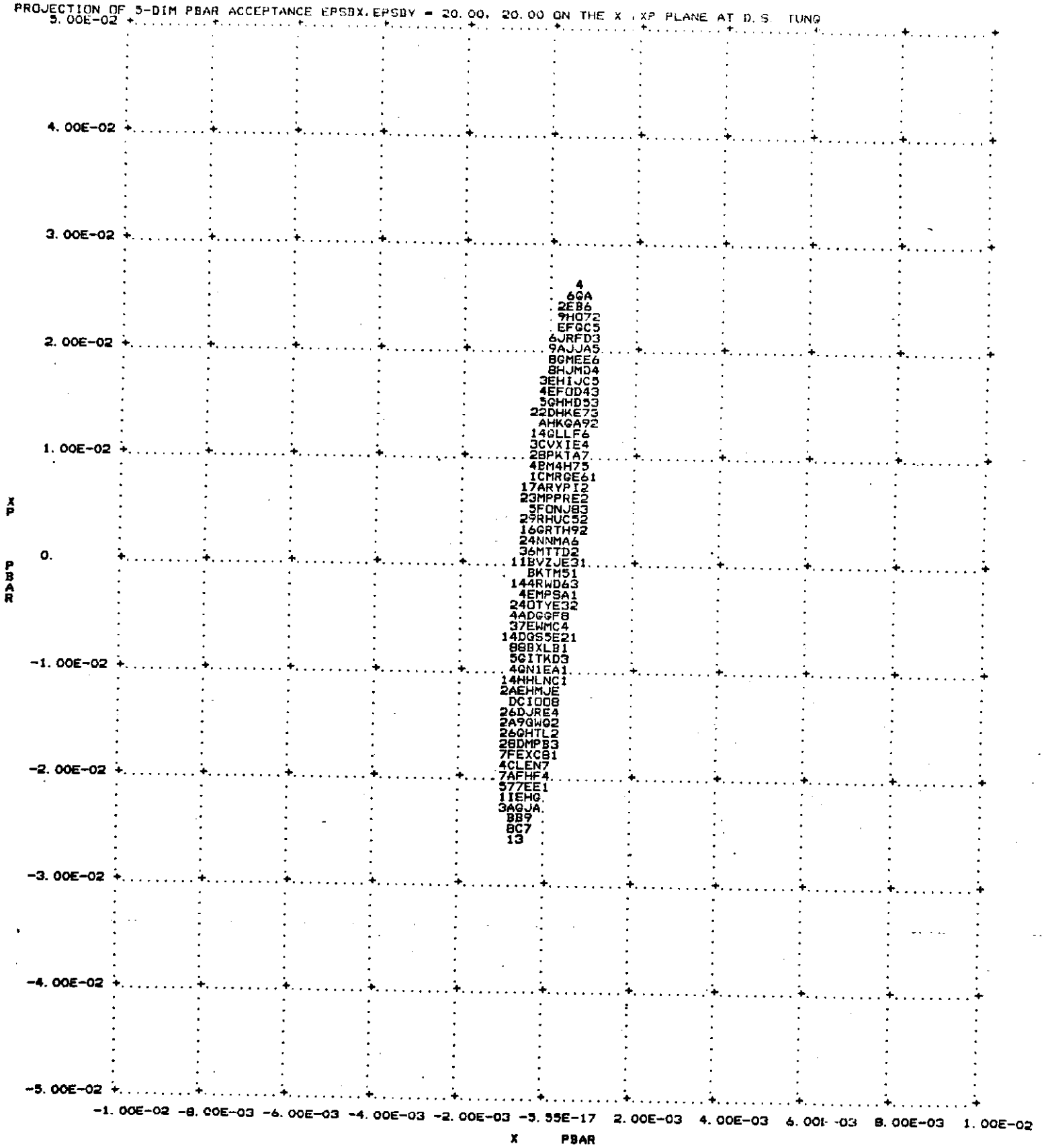
PROJECTION OF 5-DIM PBAR ACCEPTANCE EPSBX,EPSBY = 20.00, 20.00 ON THE X , XP PLANE AT D.S. TUNE
5.00E-02
4.00E-02
3.00E-02
2.00E-02
1.00E-02
0.
-1.00E-02
-2.00E-02
-3.00E-02
-4.00E-02
-5.00E-02
XP
PBAR
-1.00E-02 -8.00E-03 -6.00E-03 -4.00E-03 -2.00E-03 -5.55E-17 2.00E-03 4.00E-03 6.00E-03 8.00E-03 1.00E-02
X PBAR

Fig. 7b

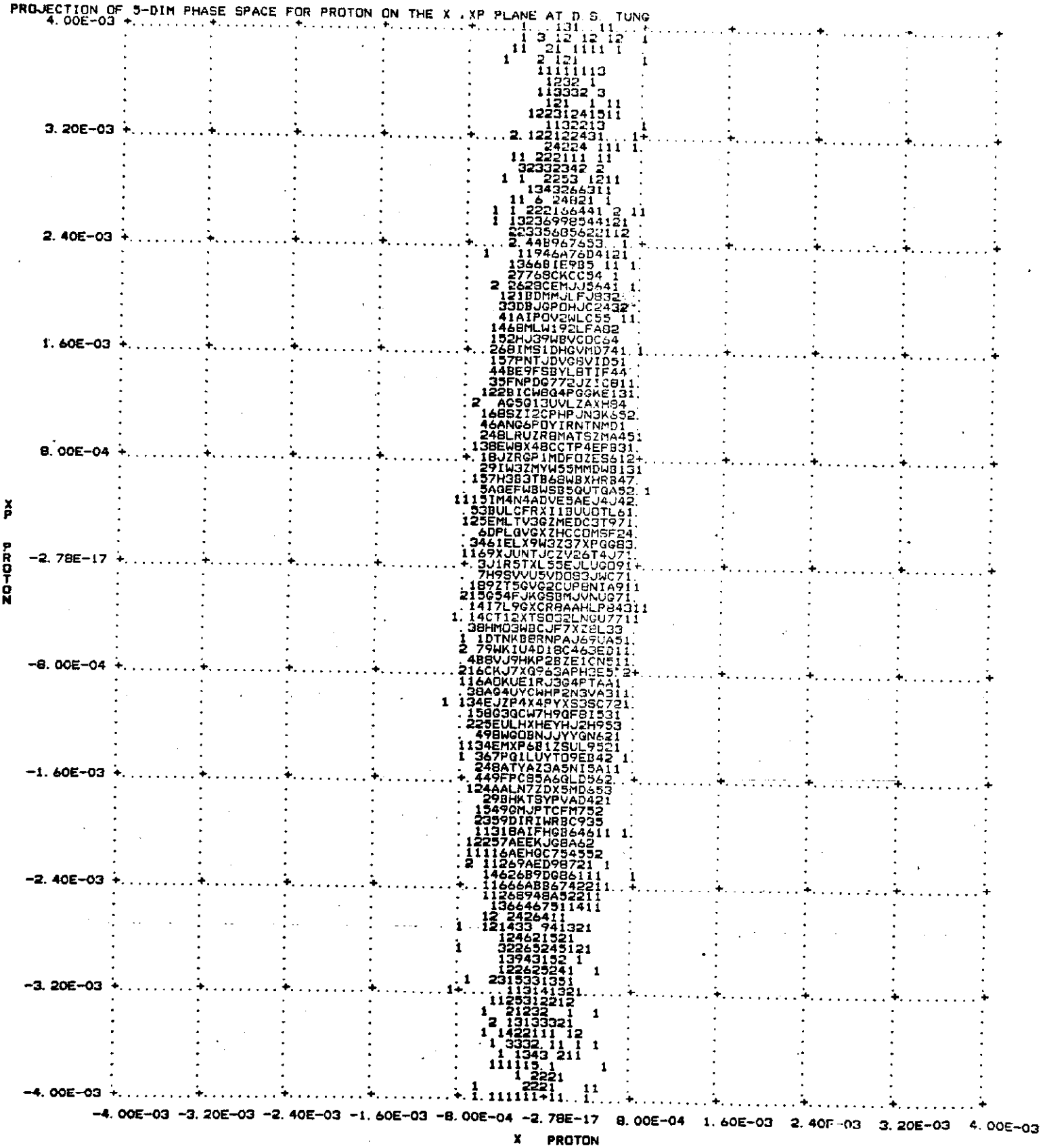
PROJECTION OF 5-DIM PHASE SPACE FOR PROTON ON THE X , XP PLANE AT D S TUNG
4.00E-03
3.20E-03
2.40E-03
1.60E-03
8.00E-04
-2.78E-17
-8.00E-04
-1.60E-03
-2.40E-03
-3.20E-03
-4.00E-03
XP PROTON
-4.00E-03 -3.20E-03 -2.40E-03 -1.60E-03 -8.00E-04 -2.78E-17 8.00E-04 1.60E-03 2.40E-03 3.20E-03 4.00E-03
X PROTON

Fig. 7c

TABLE II

YIELD FOR SEVERAL AXIALLY FOCUSED TARGET SYSTEMS

(Note: See Table I for parameters common to all entries below)

SYSTEM	# Cells	Tgt. Len. per cell [cm]	r_{target} [mm]	$\bar{k}_{target}$ [cm^{-1}]	$\bar{k}_{collector}$ [cm^{-1}]	Relative Yield	$\bar{p}$ per spill	COMMENT
A. Single Targets								
W Target Li lens coll.	1	5.5	1.0	0	.23	1.	5.1×10^{7}	Reference case
Current carrying Be target	1	20.0	0.8	10π	0.	1.27	2.6×10^{8}	Uniform current
Current carrying Be target	1	20.0	0.8	NA	0.	.87	1.8×10^{8}	Surface current
Be target	1	20.0	0.8	0	0.	.66	1.3×10^{8}	No current
Current carrying Be target	1	36.7	0.8	10π	0.	.82	1.7×10^{8}	Length=abs length
B. Multiple Targets								
Be target 11.1 cm Li lens	2	10.5	0.8	0	.14	.76	1.5×10^{8}	
Be target 11.1 cm Li lens	3	7.0	0.8	0	.14	.97	2.0×10^{8}	
Be target 11.1 cm Li lens	4	5.25	0.8	0	.14	.91	1.9×10^{8}	
C. Alternating Gradient Target Channel								
Be target 10 cm Li lens	1	5.25	1.0	-.18	.13	.53	1.1×10^{8}	
	2	5.25	1.0	-.18	.13	.81	1.6×10^{8}	
	3	5.25	1.0	-.18	.13	.97	2.0×10^{8}	
	4	5.25	1.0	-.18	.13	.80	1.6×10^{8}	